

# Manipulation of Single Neutral Atoms in Optical Lattices

Chuanwei Zhang<sup>1</sup>, S. L. Rolston<sup>2</sup>, and S. Das Sarma<sup>1</sup>

<sup>1</sup> *Condensed Matter Theory Center, Department of Physics,  
University of Maryland, College Park, Maryland, 20742 USA*

<sup>2</sup> *Department of Physics, University of Maryland, College Park, Maryland, 20742 USA*

We analyze a scheme to manipulate quantum states of neutral atoms at individual sites of optical lattices using focused laser beams. Spatial distributions of focused laser intensities induce position-dependent energy shifts of hyperfine states, which, combined with microwave radiation, allow selective manipulation of quantum states of individual target atoms. We show that various errors in the manipulation process are suppressed below  $10^{-4}$  with properly chosen microwave pulse sequences and laser parameters. A similar idea is also applied to measure quantum states of single atoms in optical lattices.

PACS numbers: 03.67.Lx, 39.25.+k, 03.75.Lm, 03.75.Mn,

## I. INTRODUCTION

Neutral atoms trapped in optical lattices are excellent candidates for quantum computation because they are well isolated from environment, leading to long coherence times, and easy to use for storing and processing quantum information [1, 2]. In optical lattices, controlled interactions between atoms may be implemented effectively, and highly entangled states of many atoms may be created in a single operational step [3, 4, 5]. More importantly, very efficient schemes for quantum error corrections [6] and fault-tolerant computing [7] can be straightforwardly implemented because of parallel operations in optical lattices [8] and long coherence times.

An outstanding challenge for quantum computation in optical lattices is the selective manipulation and measurement of quantum states of single atoms, because spatial periods of typical optical lattices are shorter than optical resolutions (long wavelength lattices may provide single site addressability, but it is difficult to implement Mott insulating states with one atom per site necessary for quantum computation in such lattices [9]). Single qubit operation is not only a building block of universal quantum computation [10], but also an essential ingredient for the recently proposed one way quantum computation, where quantum information is processed by performing single qubit rotations and measurements on entangled cluster states [11]. Experimentally, entangled cluster states have been realized for neutral atoms by using controlled cold collisions in spin-dependent optical lattices [4]. Therefore, implementations of single atom manipulation and measurement may eventually lead to universal quantum computation in optical lattices.

In this paper, we show that high fidelity selective manipulation and measurement of single atoms in optical lattices can be achieved with the assistance of focused lasers [12]. Consider a deep two dimensional optical lattice with one atom per lattice site [13]. The logical qubit basis of each atom is formed by two hyperfine states that can be coupled coherently using microwave radiation. The couplings are same for all atoms because of

the degeneracy of their hyperfine splittings. In the presence of spatially varying external fields, the degeneracy may be lifted and atoms separated by certain distance can be individually manipulated. For instance, individual atoms separated around  $2.5\mu m$  have been selectively addressed in an experiment using magnetic field gradients [14], but such a method is not useful for atoms separated by a half-wavelength of typical optical lattices, where impractically large gradients or small fluctuations of the magnetic fields would be required.

The degeneracy of hyperfine splittings may also be lifted in the presence of focused lasers that induce position-dependent energy shifts of hyperfine states (*light shifts*) [15] due to the spatial distributions of laser intensities. Through varying intensities and detunings of the focused lasers, we may adjust the difference of hyperfine splittings between neighboring atoms to a regime where microwave radiation affects mainly target atoms, while impact on non-target atoms is strongly suppressed with properly chosen microwave pulse sequences. Various errors in the manipulation process are found to be below  $10^{-4}$  except for the spontaneous emission probability of atoms in the focused laser. Finally, we show that the quantum states of individual atoms in optical lattices may also be measured using position-dependent energy shifts of hyperfine states.

## II. SELECTIVE MANIPULATION OF SINGLE ATOMS

We develop the scheme as realistically as possible, and illustrate it using  $^{87}\text{Rb}$  atoms, although the technique is applicable to other species as well. Consider  $^{87}\text{Rb}$  atoms confined in a two dimensional ( $xy$  plane) optical lattice with wavelength  $\lambda = 850nm$ . Perpendicular to the plane, the atomic dynamics are frozen out by high frequency optical traps [16]. The lattice is ramped up adiabatically to a potential depth  $V_L = 50E_r$  such that the Bose-Einstein condensate is converted into a Mott insulating state with one atom per lattice site [13]. Here  $E_r$  denotes the recoil energy  $E_r = \hbar^2 k^2 / 2m \approx \hbar \times 2\pi \times 3.18KHz$ . Two

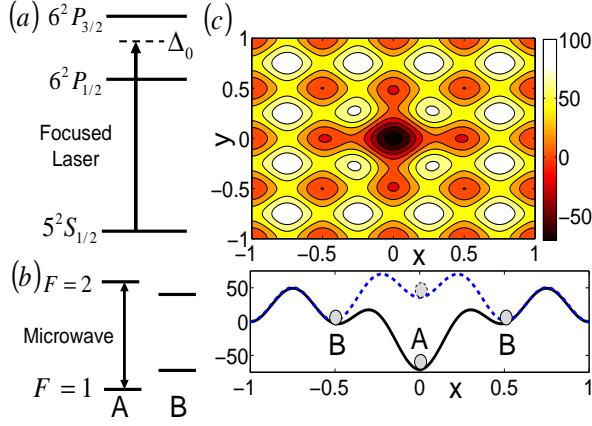


Figure 1: (color online). The scheme for manipulating single atoms in optical lattices using focused lasers and microwave radiation. (a)  $^{87}\text{Rb}$  hyperfine structure.  $\Delta_0$  is the detuning of the focused laser from the transition  $5^2S_{1/2} \rightarrow 6^2P_{3/2}$ . (b) Position-dependent hyperfine splitting induced by the spatial distribution of the focused laser intensity. Microwave radiation couples two hyperfine states of atoms. (c) Optical potentials for atoms around the focused laser. The length unit is the wavelength  $\lambda = 850\text{nm}$  of the optical lattice. The energy unit is the recoil energy  $E_r$ . Top: a 2D plot for atoms at state  $|0\rangle$ . Bottom: a 1D plot along  $y = 0$ . Solid and dashed lines for states  $|0\rangle$  and  $|1\rangle$  respectively.

hyperfine ground states  $|F = 1, m_F = -1\rangle \equiv |0\rangle$ , and  $|F = 2, m_F = -2\rangle \equiv |1\rangle$  are chosen as the logical basis of a single atom qubit at each site.

### A. Position-dependent hyperfine splittings

To manipulate a target atom  $A$ , we adiabatically turn on a focused laser that propagates along  $\hat{z}$  axis having the maximal intensity located at  $A$  (Fig.1). The focused laser is obtained by passing an initial large Gaussian beam with waist  $w$  through a lens with diameter  $D$  and focal length  $f$ , and its intensity shows an Airy pattern  $I(r) = \frac{I(0)}{G^2} \left( \int_0^{\frac{D}{2}} r' J_0 \left( k_f r' r / \sqrt{r^2 + f^2} \right) \exp(-r'^2/w^2) dr' \right)^2$ , where  $k_f = 2\pi/\lambda_f$  is the wavevector of the focused laser,  $J_0(r)$  is the zero order Bessel function, and  $G = \int_0^{D/2} r' J_0(0) \exp(-r'^2/w^2) dr'$ . With properly chosen lens parameters (see Tab I), the initial Gaussian beam is focused to the diffraction limit, where the intensity pattern is accurately described by above Airy function. In contrast, commonly used Gaussian beam approximation is not precise in such limit. In addition, the Airy pattern has a narrower waist for the central intensity distribution, leading to a smaller focused laser intensity on neighboring atoms, although the pattern extends more broadly than a Gaussian distribution that has an exponential decay.

Such an intensity pattern induces position-dependent energy shifts [17]

$$\Delta E_i(r) = \frac{3\pi c^2}{2} I(r) \sum_{j \neq i} \frac{\Gamma_j |c_{ij}|^2}{\omega_{ij}^3 \Delta_{ij}} \quad (1)$$

for hyperfine ground states  $|0\rangle$  and  $|1\rangle$ , where  $c$  is the speed of light,  $\Gamma_j$  is the decay rate of excited state  $|j\rangle$ ,  $c_{ij}$  is the transition coefficient,  $\omega_{ij}$  is the frequency, and  $\Delta_{ij}$  is the detuning of the focused laser for the transition  $|i\rangle \rightarrow |j\rangle$ . Different polarizations and detunings of the focused laser yield different shifts of hyperfine splittings  $|\Delta E(r)| = |\Delta E_1(r) - \Delta E_0(r)|$  between two qubit states. Here we choose a  $\sigma^+$ -polarized laser that drives the  $5S \rightarrow 6P$  transition [18] to obtain a small diffraction limit (Fig.1(a)). The laser induces a red-detuned trap for state  $|0\rangle$ , but a blue-detuned trap for state  $|1\rangle$ . The wavelength  $\lambda_f \approx 421\text{nm}$  (i.e. the detuning  $\Delta_0$ ) is optimized to obtain the maximal ratio between energy splitting of two qubit states and the spontaneous scattering rate [4].

Because of the inhomogeneity of the focused laser intensity,  $|\Delta E(r)|$  reaches a maximum at the target atom  $A$  and decreases dramatically at neighboring sites, as shown in Fig. 1. Therefore the degeneracy of hyperfine splittings between different atoms is lifted (Fig.1(b)). In Fig.1(c), the optical potential  $V$  for atoms around the focused laser is plotted. We see that the minimal potential barrier,  $\Delta V \approx 20E_r$ , occurs for atom  $B$  at state  $|0\rangle$ . The tunneling rate of atom  $B$  to the neighboring site  $A$  is  $\varpi \approx 2\pi J^2/\hbar E_g$  using Fermi's Golden rule, where  $J$  is the hopping matrix element and  $E_g$  is the energy gap between the initial and final states. In a symmetric optical lattice,  $E_g$  is just the on-site interaction between two atoms. The asymmetry of sites  $A$  and  $B$  yields an energy gap  $E_g$  on the order of the trapping frequency of site  $A$ , which strongly suppresses the tunneling rate. A rough estimate shows that the tunneling time  $1/\varpi$  is about 13s for the parameters in Tab. I.

To avoid excitations of atoms to higher bands of optical lattices, the rising speed of the focused laser intensity should satisfy the adiabatic condition  $\hbar |d\Delta E_i(0)/dt| = \xi |\omega_{eg}|^2 / |\langle \Phi_e | \partial V / \partial \Delta E_i(0) | \Phi_g \rangle|$ , where  $\omega_{eg}$  is the energy gap,  $|\Phi_g\rangle$  and  $|\Phi_e\rangle$  are the wavefunctions of the ground and excited states, and  $\xi \ll 1$  is a parameter

Table I: Experimental parameters.  $\delta(\lambda/2)$  is the difference of the hyperfine splittings between atoms  $A$  and  $B$ . For other atoms,  $\delta$  is slightly larger.  $\tau$  is the spontaneous emission probability for atoms in the focused laser during the single qubit manipulation process.  $P_f$  is the power of the focused laser. The recoil energy  $E_r = \hbar \times 2\pi \times 3.18\text{KHz}$ .

$\lambda$	$V_L$	$D$	$f$	$w$	$\lambda_f$	$\frac{\Delta_0}{2\pi\hbar}$
850nm	50 $E_r$	20mm	20mm	20mm	421nm	-1209GHz
$ \Delta E(0) $	$\hbar\delta(\frac{\lambda}{2})$	$\hbar\omega_0$	$\Delta V$	$\tau$	$P_f$	
107 $E_r$	102 $E_r$	12.8 $E_r$	15 $E_r$	$6 \times 10^{-4}$	17μW	

that determines the degree of adiabaticity. Because of the high potential barrier for each atom, the wavefunctions and energy gap may be obtained using the harmonic oscillator approximation, and we find  $\left| \frac{d\Delta E_i(0)/E_r}{dt} \right| = \xi \frac{8\bar{w}^2 E_r (\Delta V_i(r)/E_r)^{5/4}}{\hbar a_0 r \exp(-2r^2/\bar{w}^2)}$ , where  $a_0 = \sqrt{\hbar^2/mE_r}$ ,  $\Delta V_i(r)$  is the potential barrier for atom at position  $r$  with state  $|i\rangle$ , and we have approximated the Airy pattern of the focused laser intensity using a Gaussian function with an effective beam waist  $\bar{w}$ . The rising speed is limited by atom  $B$  at state  $|0\rangle$  that has minimal potential barrier, and is estimated to be  $\left| \frac{d\Delta E_0(0)/E_r}{dt} \right| \approx 3.6 \times 10^6 \xi (\Delta V(\lambda/2)/E_r)^{5/4} \text{Hz}$ . The total ramping up time is found to be  $57\mu\text{s}$  for  $\xi = 0.005$ , which corresponds to a  $10^{-4}$  probability for excitation to higher bands.

### B. Single qubit rotation

The position-dependent hyperfine splittings induced by the focused laser, combined with microwave radiation, can be used to perform arbitrary single qubit unitary operations on the target atom  $A$ . The microwave frequency is chosen to be resonant with the hyperfine splitting of  $A$ , and has a  $\delta(r) = (|\Delta E(0)| - |\Delta E(r)|)/\hbar$  detuning for non-target atoms (Fig. 1(b)). The coupling between two states  $|0\rangle$  and  $|1\rangle$  is described by the Rabi equation

$$i \frac{d}{dt} \begin{pmatrix} c_0 \\ c_1 \end{pmatrix} = \begin{pmatrix} 0 & e^{-i\chi}\Omega(t)/2 \\ e^{i\chi}\Omega(t)/2 & -\delta \end{pmatrix} \begin{pmatrix} c_0 \\ c_1 \end{pmatrix}, \quad (2)$$

where  $\Omega$  is the Rabi frequency and  $\chi$  is the phase of the microwave. The evolution of the quantum states is equivalent to the rotation of a spin with components  $S_z = |c_1|^2 - |c_0|^2$ ,  $S_x = 2 \cos \theta |c_1 c_0|$ ,  $S_y = 2 \sin \theta |c_1 c_0|$  on a Bloch sphere [15], where  $\theta$  is the relative phase between two states.  $\delta$  is the rotation frequency along  $\hat{S}_z$  axis, while  $\Omega(t)$  is the frequency along an axis on  $xy$  plane whose direction is determined by phase  $\chi$ . For instance,  $\chi = 0$  and  $\pi/2$  correspond to rotations along axes  $\hat{S}_x$  and  $\hat{S}_y$  respectively, and the combination of them may implement arbitrary single qubit unitary operations [1]. In this paper we focus on  $\chi = 0$  although similar results for  $\chi = \pi/2$  may be obtained straightforwardly.

To achieve a reliable single qubit rotation with negligible impact on non-target atoms, the microwave Rabi pulses need to satisfy the following criteria: (i) the variations of the occupation probabilities of state  $|1\rangle$  of non-target atoms are extremely small (below  $10^{-4}$ ); (ii) the relative phase  $\theta$  between two qubit states must return to the initial value after the microwave pulses. In the following, we show how a single qubit rotation on the target atom  $A$  satisfying these criteria is achieved by using Gaussian shaped rotation pulses together with refocusing pulses.

A Gaussian shaped pulse  $\Omega(t) = \Omega_0 \exp(-\omega_0^2 t^2)$  ( $-t_f \leq t \leq t_f$ ) is used to perform a single qubit rota-

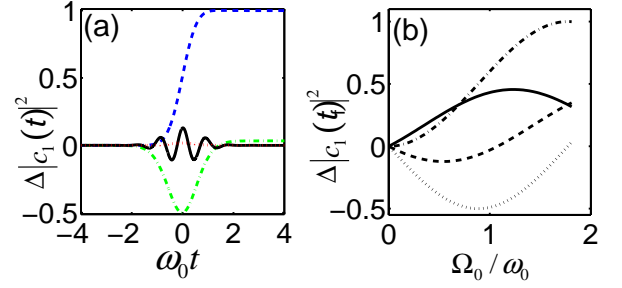


Figure 2: (color online). (a) Time evolution of  $\Delta|c_1(t)|^2$  during the microwave pulse.  $\Omega_0/\omega_0 = 1.81$  is the Rabi amplitude for a pulse whose area is slightly larger than  $\pi$ . Atoms  $A$  (dashed dotted) and  $B$  (solid) with initial state  $(c_0, c_1) = (\sqrt{1/2}, i\sqrt{1/2})$ ; atoms  $A$  (dashed) and  $B$  (dotted) with initial state  $(1, 0)$ . (b)  $\Delta|c_1(t_f)|^2$  is the population variation of atom  $A$  after the microwave pulse. Initial states  $(1, 0)$  (dashed dotted);  $(\sqrt{1/2}, i\sqrt{1/2})$  (dotted),  $(\sqrt{2/3}, \sqrt{1/4} + i\sqrt{1/12})$  (dashed), and  $(\sqrt{2/3}, \sqrt{1/4} - i\sqrt{1/12})$  (solid).

tion on the target atom  $A$ . In the frequency domain, the Fourier transformation  $\Omega(\omega)$  of the Rabi frequency  $\Omega(t)$  of this type of pulse shows a Gaussian shaped decay with respect to the detuning  $\delta$  from the microwave frequency. Because of their large detuning  $\delta$ , non-target atoms undergo Rabi oscillations with small frequencies  $\Omega(\delta)$ , which strongly suppress the variations of their occupation probabilities.

This scenario is confirmed by numerically integrating Eq. (2) with different initial states and calculating the variation  $\Delta|c_1(t)|^2 = |c_1(t)|^2 - |c_1(-t_f)|^2$  of the occupation probabilities at state  $|1\rangle$ . A small constant  $\omega_0 = \frac{1}{8}\delta(\frac{\lambda}{2})$  for the microwave is chosen to avoid large impact on non-target atoms, and different pulse areas are implemented by varying the pulse amplitude  $\Omega_0$ , instead of the pulse period  $2t_f$ . In Fig. 2(a),  $\Delta|c_1(t)|^2$  of atoms  $A$  and  $B$  are plotted with respect to the scaled time  $\omega_0 t$ . We see large variations of  $|c_1|^2$  for atom  $A$  after the pulse, which correspond to a single qubit rotation. In comparison, there are no obvious changes of  $|c_1|^2$  for the neighboring atom  $B$ . In Fig. 2(b), the total changes of  $|c_1|^2$  for the target atom  $A$  at time  $t_f$  are plotted with respect to  $\Omega_0/\omega_0$ . We see different pulse areas can be achieved by adjusting  $\Omega_0$ .

For the target atom ( $\delta = 0$ ), the time evolution of  $|c_1(t)|^2$  can be obtained analytically by solving Eq. (2), which yields

$$|c_1(t)|^2 = (1 - \rho \sin(\eta\Omega_0/\omega_0 + \phi))/2. \quad (3)$$

Here  $\rho = \sqrt{1 - 4|c_0(-t_f)|^2|c_1(-t_f)|^2 \cos^2 \theta(-t_f)}$ ,  $\eta = \omega_0 \int_{-t_f}^t \exp(-\omega_0^2 t'^2) dt'$  and  $\phi = \arcsin\left(\left(1 - 2|c_1(-t_f)|^2\right)/\rho\right)$ . This expression is

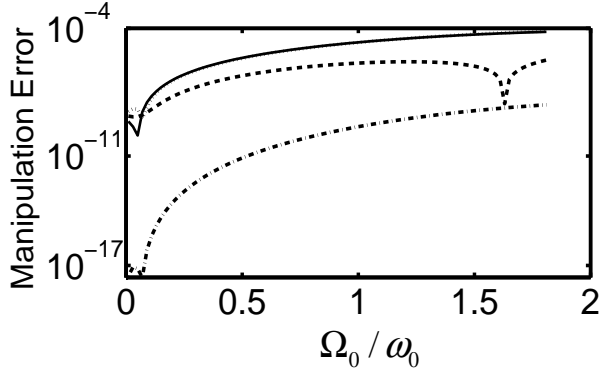


Figure 3: Manipulation error  $\epsilon = ||c_1(t_f)|^2 - |c_1(-t_f)|^2|$  for the nearest neighboring atom  $B$ .  $\epsilon$  is smaller for other atoms because they have larger detuning  $\delta(r)$ .  $-7 \leq \omega_0 t \leq 7$  in the numerical integration of Eq. (2). Initial states are same as those in Fig. 2(b).

in very good agreement with the numerical results presented in Fig. 2. In Fig. 3, we plot the single qubit manipulation errors for the nearest neighboring atom  $B$  with respect to  $\Omega_0/\omega_0$ . The errors are smaller than  $10^{-4}$  for different Rabi pulse areas and different initial states. We have also performed numerical simulations for many other initial states, finding that errors below  $10^{-4}$  are always achieved. The manipulation errors are even smaller for all other atoms because they have larger detuning  $\delta(r)$ .

The relative phase  $\theta$  is harder to control than the occupation probability because it can not only vary from 0 to  $2\pi$  many times with large frequency  $\delta(r)$  during the Rabi pulses, but also be easily affected by interactions with the environment that lead to dephasing. To eliminate the variation of  $\theta$ , we use the following pulse sequence that is similar to the refocusing process in NMR studies [1]. To realize an area  $\alpha$  pulse, we adiabatically ramp up the focused laser, apply a  $\alpha/2$  pulse on the target atom  $A$  (it induces a rotation around  $\hat{S}_x$  axis) using the Gaussian shaped pulse described above, then adiabatically ramp down the focused laser in step (i). In this step, atoms obtain phase variations  $\Delta\theta$  determined by their detunings  $\delta(r)$  and the dephasing process. In step (ii), we apply a fast resonant  $\pi$  pulse to all atoms that corresponds to an angle  $\pi$  rotation around  $S_x$  axis. This pulse is called the refocusing pulse. In step (iii) we repeat step (i), and in step (iv) we apply another  $\pi$  refocusing pulse. The two refocusing pulses do not affect the pulse area for target atoms because the combination of them corresponds to a  $2\pi$  rotation around  $S_x$  axis. However, the effective directions of the rotations around  $S_z$  axis for all atoms in step (iii) are reversed from that in step (i) by two refocusing pulses, therefore the phase variation in step (iii) becomes  $-\Delta\theta$ . These two phase variations cancel each other and the relative phase  $\theta$  returns to its initial value after the pulse sequence.

### C. Fidelity analysis

In an experiment, a difficult parameter to specify is the spatial distribution of the focused laser intensity that determines the detuning  $\delta(r)$ , the central parameter of the scheme. However, our scheme only requires a large  $\delta(r)$ , not any specific value, therefore this is not a significant difficulty. Another important issue in the experiment is the misalignment of the focused laser from the minimum of the optical lattice potential. A small displacement  $\Delta x$  of the focused laser induces a detuning of the microwave scaling as  $(\Delta x)^2$  from the hyperfine splitting between two qubit states of the target atom, and thus reduces the fidelity of the single qubit rotation. For  $\Delta x = 1nm$ , we estimate the detuning to be  $2\pi \times 3Hz$  and the fidelity of the single qubit rotation is degraded by  $2 \times 10^{-4}$ . Generally, errors due to small mis-detuning of the microwave may be corrected using composite pulses technology developed in the NMR quantum computation [19].

In the single qubit manipulation, the probability of spontaneous scattering one photon for atoms in the focused laser is estimated to be  $\tau = 6 \times 10^{-4}$ , which is the worst parameter in the scheme. This parameter is limited by the need for a maximal ratio between the vector light shifts and the spontaneous scattering rate, which does not allow arbitrarily large detunings.

### III. SELECTIVE DETECTION OF SINGLE ATOMS

The energy shift induced by the focused laser is around several hundreds  $KHz$ , which is much smaller than the decay rate  $\Gamma$  of excited states and cannot be used to selectively measure quantum states of target atoms. To obtain large energy shifts, we transfer the target atom to other magnetic sublevels ( $|0\rangle \rightarrow |\bar{1}\rangle \equiv |F=2, m_F=2\rangle$ ,  $|1\rangle \rightarrow |0\rangle$ ) using several  $\pi$  microwave pulses with the assistance of focused lasers. Then a focused  $\sigma^+$ -polarized laser resonant with the transition  $|\bar{1}\rangle \rightarrow |6^2P_{3/2} : F'=3, m'_{F'}=3\rangle$  is applied to detect atoms at state  $|\bar{1}\rangle$ . In this process, resonant fluorescence is observed if and only if the initial state of the target atom is  $|0\rangle$  and the probability to detect an atom yields  $|c_0|^2$  of the target atom. The detection laser can be focused on the target atoms as well as the focused laser beam using for single atom manipulation because they both use  $5S \rightarrow 6P$  transition. In the experiment, a constant  $30G$  magnetic field along  $x$ -axis may be used to induce about  $2\pi \times 84MHz$  Zeeman splitting between states  $|1\rangle$  and  $|\bar{1}\rangle$ , while  $2\pi \times 111.6MHz$  between  $|6^2P_{3/2} : F'=3, m'_{F'}=-1\rangle$  and  $|6^2P_{3/2} : F'=3, m'_{F'}=3\rangle$  [15]. Therefore the detection laser is about  $\delta_1 = 2\pi \times 27.6MHz$  detuned from the transition  $|1\rangle \rightarrow |6^2P_{3/2} : F'=3, m'_{F'}=-1\rangle$ , which yields a maximal ratio  $(\Gamma_1/2\delta_1)^2 I(r)/I(0) \lesssim 2 \times 10^{-5}$  [15] between the photons scattering on non-target and target atoms, that is,  $5 \times 10^4$  photons have been scattered

on the target atoms to induce one photon scattering on the neighboring non-target atoms. The impact on non-target atoms in the detection process may therefore be neglected.

#### IV. DISCUSSION AND CONCLUSION

We emphasize that such high fidelity single atom manipulation cannot be accomplished using magnetic field gradients. To obtain the same detuning  $\delta(r)$  as that using focused lasers, an impractical magnetic field gradient ( $\sim 3.6\text{T/cm}$ ) is required. While in a typical gradient  $10\text{G/cm}$ , a single atom rotation takes about  $40\text{ms}$  (much longer than the cold collision time ( $\sim 100\mu\text{s}$ ) for many-qubit gates [3, 4]), and requires unattainably small magnetic field fluctuations ( $\sim 10^{-6}\text{G}$ ). In addition, the magnetic field gradient method can only be used to selectively address atoms along one dimension, while the focused laser scheme can select two dimensions.

We notice that single qubit rotations may also be performed using two-photon Raman transitions [20] with the assistance of focused lasers. In this case, the beam waists of the Raman pulses need to be relatively large ( $\sim 2\mu\text{m}$ ) so that small misalignments of the lasers do not cause large changes of the laser intensities on the target atoms that may diminish the fidelity of single qubit rotations. Because two-photon Raman transitions only affect atoms

inside the Rabi pulses, atoms separated by a long distance may be addressed simultaneously with different pulse sequences, which may reduce the total computation time.

In summary, we have analyzed a scheme for manipulating and measuring quantum states of single atoms in optical lattices with the assistance of focused lasers. With properly chosen experimental parameters, various manipulation errors are suppressed below  $10^{-4}$  except the spontaneous emission probability of atoms in focused lasers. Our proposal includes a realistic and practical quantitative analysis suggesting plausible experimental implementation of single atom manipulation in optical lattice quantum computation architecture. The technique also has broad applications for investigating various interesting physics in optical lattices such as engineering and probing many-body quantum states in strongly-correlated systems, topological quantum computation, etc. [21]. We believe that our work establishes a practical and workable method for single atom manipulation in optical lattices.

#### Acknowledgments

We thank V. Scarola for valuable discussion. This work is supported by ARO-DTO, ARO-LPS, and NSF.

- 
- [1] M.A. Nielsen, and I.L. Chuang, *Quantum computation and quantum information*, (Cambridge University Press, Cambridge 2000).
  - [2] P. Zoller, *et al.*, arXiv: quant-ph/0405025.
  - [3] D. Jaksch, *et al.*, Phys. Rev. Lett. **82**, 1975 (1999).
  - [4] O. Mandel, *et al.*, Phys. Rev. Lett. **91**, 010407 (2000); Nature **425**, 937 (2003); O. Mandel, PhD dissertation.
  - [5] L.-M. Duan, E. Demler, and M.D. Lukin, Phys. Rev. Lett. **91**, 090402 (2003).
  - [6] A.M. Steane, Rep. Prog. Phys. **61**, 117 (1998).
  - [7] P.W. Shor, Phys. Rev. A **52**, R2493 (1995).
  - [8] H.J. Briegel, *et al.*, J. Mod. Opt. **47**, 415 (2000).
  - [9] R. Scheunemann, *et al.*, Phys. Rev. A **62**, 051801(R) (2000); D.S. Weiss, *et al.*, *ibid* **70**, 040302(R) (2004); J. Vala, *et al.*, *ibid* **71**, 032324 (2005).
  - [10] A. Barenco, *et al.*, Phys. Rev. A **52**, 3457 (1995).
  - [11] R. Raussendorf and H.J. Briegel, Phys. Rev. Lett. **86**, 5188 (2001).
  - [12] S.L. Rolston, in *Proceedings of the 1st International Conference on Experimental Implementation of Quantum Computation*, (Rinton Press, Princeton, 2001).
  - [13] M. Greiner, *et al.*, Nature **415**, 39 (2002).
  - [14] D. Schrader, *et al.*, Phys. Rev. Lett. **93**, 150501 (2004).
  - [15] H.J. Metcalf, and P. van der Straten, *Laser cooling and trapping*, (Springer-Verlag, New York 1999).
  - [16] T. Meyrath, *Opt. Express* **13**, 2843 (2005).
  - [17] P.S. Jessen and I.H. Deutsch, Adv. At. Mol. Opt. Phys. **37**, 95 (1996).
  - [18] Only transitions to  $6P$  states are considered because the detunings to other states are much larger.
  - [19] H.K. Cummins, *et al.*, Phys. Rev. A **67** 042308 (2003).
  - [20] D.D. Yavuz, *et al.*, Phys. Rev. Lett. **96**, 063001 (2006).
  - [21] C. Zhang, *et al.*, to be published.